Journal of Power Sources 195 (2010) 883–889

Contents lists available at ScienceDirect

Journal of Power Sources

journal homepage: www.elsevier.com/locate/jpowsour

Examination of different lattice structures in porous electrodes using a three-dimensional conductivity model

Song Zhang, Thomas Bean*, Dean B. Edwards

University of Idaho, Moscow, ID 83844-0902, USA

ARTICLE INFO

Article history:
Received 12 July 2009
Received in revised form 10 August 2009
Accepted 11 August 2009
Available online 19 August 2009

Keywords:
Lead acid battery
3D model
Porous electrode
BCC and FCC lattice structures

ABSTRACT

In this paper a three-dimensional (3D) conductivity model previously developed for a porous electrode having a simple cubic lattice structure is expanded to include other lattice structure types. The other structures analyzed are the extended simple cubic (XSC), body centered cubic (BCC), and face centered cubic (FCC) lattices. As in the previous paper, we model the 3D lattice of nodes as identical spheres in electrical contact with each of its neighbors, and calculate the micro-porosity (i.e. the space between the spheres) for each of the three lattice structures. We use these theoretical derivations to analyze positive electrodes in lead acid batteries. We calculate the macro-porosity (i.e. porosity created by vacant node elements) needed to achieve a 50% total porosity for a lead acid positive electrode whose porosity distributions had been experimentally determined previously by other researchers. When the theoretical micro-porosities are compared to the experimentally determined porosity distributions, the sphere size for each of the lattice arrangements can be estimated. In addition, we estimate the critical volume faction (CVF) which is the maximum utilization of the positive electrode's active material for each lattice type. For these different lattice structures, the estimated node sizes vary from 1 to 10 μm and the critical volume fraction vary from 59% (SC) to 67% (XSC). An important result of this work is that the critical volume fractions for the physically realizable structures (i.e. SC, BCC, and FCC) are all very close to 60% which is the CVF for the 2D conductivity model.

1. Introduction

The utilization of an electrode is defined as the fraction of the stoichiometric capacity of the active material that reacts. According to Bode [1], the highest experimental utilization of the lead dioxide (PbO_2) to lead sulfate ($PbSO_4$) reaction in the positive plate is about 55% even at very low discharge rates. Bode [1] gives a slightly higher value of 60% for the utilization of lead (Pb) to lead sulfate ($PbSO_4$) reaction in the negative plate.

The cause of incomplete reaction in lead acid batteries has been the topic of study for many researchers. Metzendorf and his co-workers [2,3] attributed this phenomenon to the conductivity change of the active material that occurs during the discharge process. Lead (Pb) and lead dioxide (PbO_2) are conductive, whereas lead sulfate ($PbSO_4$) is nonconductive. The conductivity of the whole system changes dramatically from being conductive to nonconductive when a sufficient amount of active material is reacted. The lead sulfate electrically isolates some of the active material and prevents it from being discharged. Metzendorf showed that the powder mixture of the active material (PbO_2 and Pb) and discharge product ($PbSO_4$) could be modeled theoretically as statistically distributed networks, and this binary mixture system could be studied with the percolation theory (PT) [4] or effective medium theory (EMT) [5]. Other researchers [6] have suggested that the positive active material (PbO_2) has been treated as a gel–crystal system. Crystal zones are built of PbO_2 and exhibit electron conductivity. Gel zones are composed of hydrated lead dioxide, $PbO(OH)_2$, that forms linear polymer chains. This gel–crystal structure is used to help explain some of the electrochemical behavior of the positive electrode in a lead acid battery.

A two-dimensional (2D) conductivity model [7] and later three-dimensional models [8,9,10] were developed in order to study the effect that size and aspect ratio of conductive and/or nonconductive additives have on the utilization of lead acid batteries. The model consists of electrically connected nodes to represent the active material both before and after the discharge reaction. The nodes were assumed to be conductive, with zero resistance, before reaction and nonconductive, with infinite resistance, after reaction. If a conductive pathway could be found from a particular node to the edge of a plate, then the node was classified as dischargeable, and subsequently discharged. If no conductive pathway exists, then the node was classified as isolated and could not be discharged. At the end of the simulated discharge, all nodes would either be clas-

* Corresponding author at: University of Idaho, BEL W3-1, Moscow, ID 83844-1023, USA. Tel.: +1 208 885 4114; fax: +1 208 885 6840.
E-mail address: thomasbean@vandals.uidaho.edu (T. Bean).

0378-7753/$ – see front matter © 2009 Elsevier B.V. All rights reserved.
doi:10.1016/j.jpowsour.2009.08.026

Nomenclature

PF	packing factor (dimensionless)
r	sphere radius (m)
r_{xsc}	sphere radius in XSC lattice structure (m)
r_{bcc}	sphere radius in BCC lattice structure (m)
r_{fcc}	sphere radius in FCC lattice structure (m)
R	pore radius (m)
R_{xsc}	pore radius in XSC lattice structure (m)
R_{bcc}	pore radius in BCC lattice structure (m)
R_{fcc}	pore radius in FCC lattice structure (m)
V_c	volume of a cell (m^3)
V_p	volume of a pore (m^3)
V_s	volume of a sphere (m^3)
z	coordination number or number of contacts or pathways (dimensionless)
ε_F	final porosity (dimensionless)
ε_μ	micro-porosity (dimensionless)
ε'_M	adjusted macro-porosity (dimensionless)

sified as discharged or isolated, and the utilization was found from the fraction of the nodes that were discharged.

The coordination number z is defined as the number of contacts or pathways that one node has with its neighbors. Early research [3] suggested that for the Pb and PbO_2 electrodes, the coordination number z is approximately eight (i.e. $z \approx 8$). In a previously developed 2D conductivity model [7], the conductive pathways were horizontal, vertical, and diagonal so that the configuration had a coordination number $z = 8$. For the simple cubic (SC) 3D model [8,9,10], z has a value of six.

Although these models simulated the electronic behavior of the electrodes, they did not attempt to account for porosity. According to Bode [1], the porosity of typically charged plates is near 50%. So, how does one represent 50% porosity in one of these models? If the porosity is accommodated by simply removing half of the nodes, then the electrode utilization would be very low and inconsistent with experimental data. The approach taken in this and a previous paper [9] is that nodes are modeled as spheres with a characteristic dimension, r (see Fig. 1). When modeled in this manner, porosity exists between the spheres, which we call "micro-porosity." The remaining porosity, referred to in this paper as "macro-porosity," is achieved by eliminating spheres and disrupting the structure.

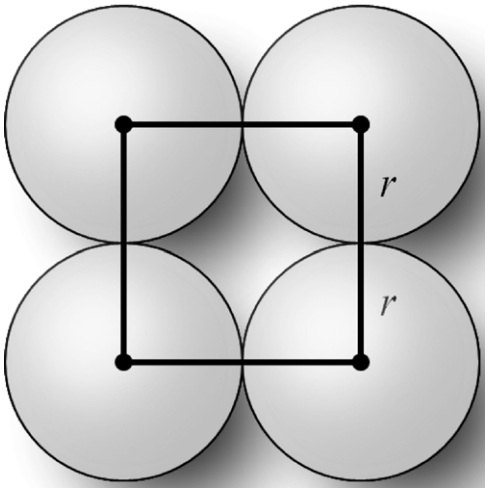

Fig. 1. Micro-porosity between spheres in a simple cubic structure.

Accounting for porosity with the 2D model is particularly troublesome. In the 2D model, the critical volume fraction (CVF) for $z = 8$ is about 60% [7]. The 2D micro-porosity is defined as the difference in area between a square and an inscribed circle which is approximately 23%. Because the porosity of an electrode is around 50%, an additional 27% of macro-porosity, which is defined as the porosity that occurs from having missing nodes for the 2D case, is required. If this additional porosity is included in the 2D analysis, the critical volume fraction (CVF) would not be 60% but approximately 33%. This is, of course, much lower than the observed values of 55–60%. A three-dimensional model must therefore be used to accurately account for porosity.

In the three-dimensional conductivity models previously discussed [8,9,10], the simple cubic (SC) node structure having coordination numbers of $z = 6$ was presented. In this paper, we will present the simulation results from three other lattice structures; the extended simple cubic (XSC), the body centered cubic (BCC), and the face centered cubic (FCC) structures, with coordination numbers $z = 10$, 8, and 12, respectively. We will calculate the appropriate micro- and macro-porosities for each structure, and estimate the sphere diameter using published pore distribution data from other researchers. We will compare the modeled utilizations with those found experimentally.

2. Model description

Although the emphasis of this paper and the example provided deals with analyzing the positive electrode of lead acid batteries, the derivation of these theoretical models is independent of the electrochemical system. The models only differentiate between different lattice structures. These structures consist of electrically conductive nodes all having the same size connected together in the specified arrangement of the lattice. As the electrode undergoes a reaction, these nodes change from being conductive to nonconductive. The extent to which this theoretical model can be applied to a given electrode is dependent on the specific characteristics of that electrode. However, many electrodes do have crystalline structures that undergo conductivity changes during the reaction so our models may be applicable to these systems. The models do predict the performance of the positive electrode in lead acid batteries but other electrodes would need to be evaluated on a case by case basis to determine their general validity.

One assumption of the model used in this paper is that all the spheres are the same size. A scanning electron microscope (SEM) picture of a lead acid positive electrode (Fig. 2) shows that the size of the particles vary as does the size of the pores in the positive active material. Our model is therefore a simplification of the complex geometry of the solid and liquid phases that exist in a real electrode. However, the abstraction that electrode structures can be modeled with a three-dimensional structure having a single sphere size provides physical insight into both the nature and types of porosity found in electrodes. Our model also provides some quantitative results that can be compared with experiments. This paper is therefore another step in our attempts to develop better conductivity models for porous electrodes where porosity is also considered in the analysis.

In this section we analyze a 3D extended simple cubic (XSC) with a coordination number of $z = 10$, a 3D body centered cubic (BCC) lattice structure with $z = 8$, and a 3D face centered cubic (FCC) structure with $z = 12$. The geometry of these lattice structures is described. After the lattice structures are described, their micro-porosities are determined. Because the node size is assumed to be the same throughout the structure, the pore size associated with the micro-porosity is also constant throughout the structure and the relationship between the micro-porosity pore size and node

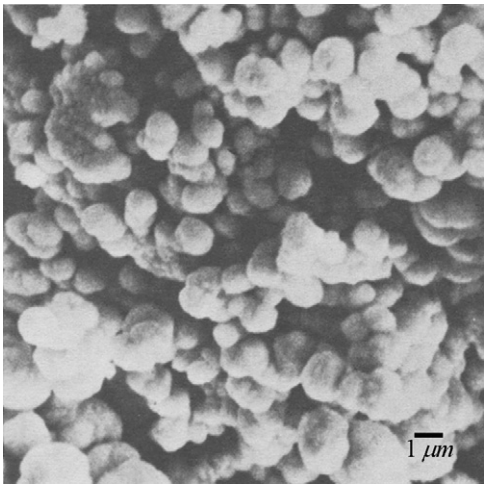

Fig. 2. Surface of a positive plate fully formed and charged, β-PbO_2. Magnification 1:4600 [1].

size can be calculated. In the next section, we calculate the generic relationship between micro-porosity pore size and node size. The results of this study including the packing factor, micro-porosity, macro-porosity and the accompanying sphere to pore ratio are tabulated in Table 1 found in Section 2.5.

2.1. Relationship between pore and node size

The micro-porosity of a lattice structure can be calculated by comparing the volume of the spheres inside a cubic cell with the volume of the cell. The packing factor of a lattice structure, *PF*, is defined as the fraction of the cell occupied by the spheres and is found by:

$$PF = \frac{nV_s}{V_c} \tag{1}$$

where n is the number of spheres in the cubic cell volume, V_c, and V_s is the volume of the sphere. The micro-porosity, ε_μ, is the empty space found around the spheres. The micro-porosity is calculated with:

$$\varepsilon_\mu = 1 - PF = 1 - \frac{nV_s}{V_c} \tag{2}$$

In this paper, it is assumed that there is one pore for each node in the idealized model presented. If the pore volume is modeled as spheres, then the relationship between sphere size and pore size can be found:

$$PF = \frac{V_s}{V_s + V_p} = \frac{(4/3)\pi r^3}{(4/3)\pi r^3 + (4/3)\pi R^3} = \frac{r^3}{r^3 + R^3} \tag{3}$$

with V_s as the sphere volume, V_p as the pore volume, r as the sphere radius and R as the pore radius. We can rearrange Eq. (3) into an expression for the sphere radius, r:

$$r = \sqrt[3]{\frac{PF}{1 - PF}}R \tag{4}$$

We see that the relationship between the pore and the sphere is only a function of the packing factor, *PF*.

2.2. Extended simple cubic lattice structure

The 3D extended simple cubic lattice structure with a coordination number of ten, i.e. $z = 10$, is shown in Fig. 3b. For comparison, we see in Fig. 3a that a simple cubic structure has a coordination number $z = 6$. The difference is there are eight nodes connected to the particular node in the same layer, four nearest nodes (directly connected) as in the simple cubic structure and four next to the nearest nodes (diagonally connected). Additionally, there are two nodes in the two immediate adjacent layers, one above and one below the current layer. The extended simple cubic (XSC) structure is not realizable in the real world. This is due to the longer distance to the diagonally connected node when compared to the directly connected node. We include this structure for comparison only. In all respects except for coordination number, it is identical to the simple cubic structure.

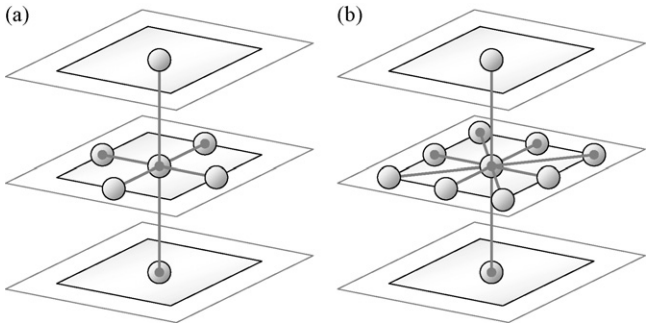

Fig. 3. Comparison of (a) 3D simple cubic ($z = 6$) and (b) 3D extended simple cubic ($z = 10$) lattice structures.

If the radius of each node shown in Fig. 3 is given as r, then the total volume of a cell V_c is equal to $8r^3$. The packing factor of an extended simple cubic lattice is:

$$PF_{sc} = \left(\frac{nV_s}{V_c}\right)_{sc} = \frac{1 \cdot (4/3)\pi r^3}{8r^3} = \frac{\pi}{6} \Rightarrow 52\% \tag{5}$$

The vacant volume percentage or micro-porosity in an undisturbed XSC lattice structure is approximately 48%. The relationship between the sphere radius and pore radius is a function of the packing factor for the XSC lattice structure. Eq. (4) provides that the sphere radius is 1.032 times larger than the pore radius, or $r_{xsc} \approx 1.032R_{xsc}$, which is the same result as for the simple cubic (SC) structure [9].

2.3. Body centered cubic lattice structure

In the BCC structure, there is one node at each corner and one node in the center of the cube as shown in Fig. 4a. Each corner node touches the central node along the body diagonal of the cube. The central node is not located in the same layer as the eight adjacent nodes as shown in the connection diagram in Fig. 4b. In other words, four neighbor nodes are located one half layer above the central node, and another four neighbor nodes are a half layer below the central node.

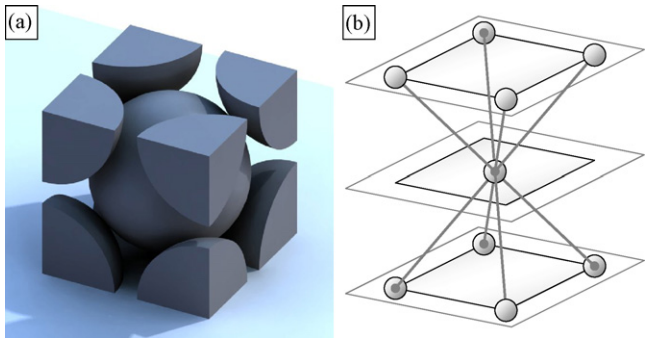

Fig. 4. 3D body centered cubic ($z = 8$) lattice structure.

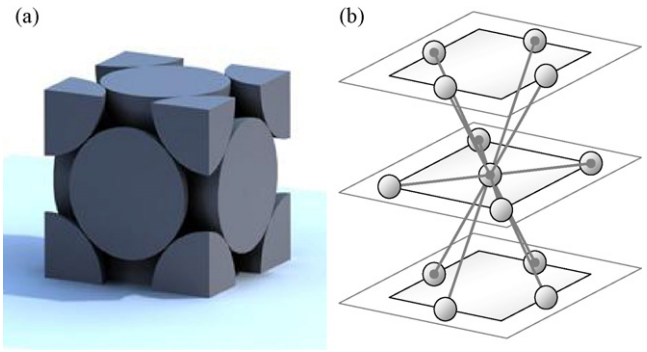

Fig. 5. 3D face centered cubic ($z = 12$) lattice structure.

The body centered cubic structure is a cube (all sides of the same length and all face perpendicular to each other) with a node at each corner of the unit cell, and a node in the center of the unit cell. The micro-porosity for the body centered cubic crystal lattice structure $z = 8$, can be calculated as follows: the radius of each sphere is given as r so that the volume of a cell V_c is equal to $(4r/\sqrt{3})^3$. The total volume of nodes in the cell V_c is $2 \cdot (4/\sqrt{3})\pi r^3$. The packing factor of a body centered cubic lattice is:

$$PF_{bcc} = \left(\frac{nV_s}{V_c}\right)_{bcc} = \frac{2 \cdot (4/\sqrt{3})\pi r^3}{\left(4r/\sqrt{3}\right)^3} = \frac{\pi\sqrt{3}}{8} \Rightarrow 68\% \quad (6)$$

The vacant volume percentage or micro-porosity in an undisturbed BCC lattice structure is approximately 32%. As with XSC, we use Eq. (4) to calculate that the sphere radius is 1.286 times larger than the pore radius, or $r_{bcc} \approx 1.286 R_{bcc}$.

2.4. Face centered cubic lattice structure

In the face centered cubic structure, as demonstrated in Fig. 5a, there is one node at each corner and one node in each face. Each corner node contributes one-eighth of its volume to the unit cell interior, and each face node contributes one-half of its volume to the unit cell interior. From Fig. 5b, we see that the face centered cubic structure has a coordination number $z = 12$. The FCC structure as represented in Fig. 5a has no central node. The connection diagram in Fig. 5b, which orients all nodes to a centered node, is also an accurate representation of the FCC structure.

In the FCC structure, if the radius of a node is given as r, then the length of a unit cell is $4r/\sqrt{2}$. Since there are four full nodes per FCC unit cell, the total FCC node volume is four times the volume of a sphere, which is $4\pi r^3/3$. Then the packing factor for the FCC structure is:

$$PF_{fcc} = \left(\frac{nV_s}{V_c}\right)_{fcc} = \frac{4 \cdot 4\pi r^3/3}{\left(4r/\sqrt{2}\right)^3} = \frac{\pi\sqrt{2}}{6} \Rightarrow 74\% \quad (7)$$

The vacant volume percentage or micro-porosity in an undisturbed FCC lattice structure is approximately 26%. Once more using Eq. (4), the size relationship between the sphere radius and pore radius is calculated to be $r_{fcc} \approx 1.418 R_{fcc}$ for the FCC structure.

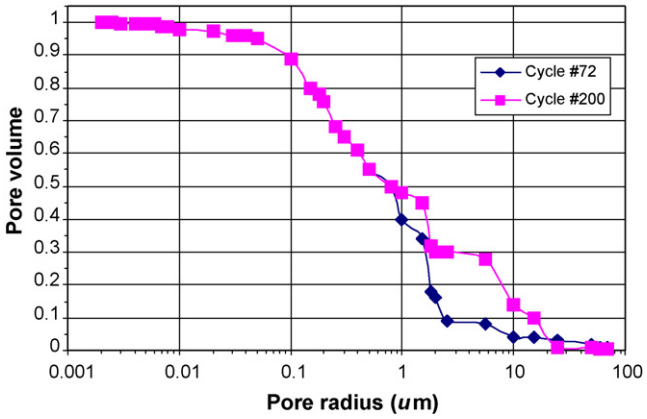

Fig. 6. Pore size distribution of plates having PbCaSn grids, slow charge [13].

2.5. Summary of porosities

Table 1 provides a summary of the parameters associated with the different lattice structures previously discussed in this section. The two parameters we are most interested in determining are micro-porosity and the ratio of the node size to the pore size. Because in our analysis we assume 50% porosity for the electrode, the macro-porosity is simply 50% minus the micro-porosity. Because the lattice structure and its geometry are independent of node size, these relations are valid for structures having nanometer-size nodes as well as structures having the size of boulders. The pore and node sizes must be established experimentally as explained in the next section.

3. Node size and macro-porosity determination from experimental data

A porous body of an electrode consists of a solid framework that is transected by a system of three-dimensional, interconnected capillaries or intermediate pores that are usually uniformly distributed throughout the interior of the electrode. The capillaries or pores that form the void volumes within the electrode are described by their average pore radius R. The method of measuring the porosity of an electrode, such as the BET method [1], the use of glycerol [11], and the influence of paste composition and curing processes on the porosity have been reported by other researchers. [12,13]

The overall porosity of the electrode, which ranges from 45% to 65% [12], is determined mainly by the different paste composition, curing and formation procedures. For the cured and formed positive plate, which is considered in this paper, we assumed that the porosity of the plate before discharge is 50%. The pore size distribution for different grid alloy and charge methods has been reported by other researchers [12,13]. In Fig. 6 [13], the pore size distribution results for plates with PbCaSn grids are shown. This figure shows, for example, that after 72 cycles a battery with a PbCaSn grid and a slow discharge (15 h discharge rate), 40% of the total pore volume consist of pores having a diameter equal to or greater than 1 μm.

For a given lattice structure, we can now estimate the sphere size from the pore radius where the porosity of the electrode is equal

Table 1
Geometric parameters for different lattice structures.

Lattice structure	Coord. number (z)	Packing factor (PF)	Micro-porosity (ε_μ)	Macro-porosity (ε'_M)	Sphere/pore size ratio (r/R)
Simple cubic	6	52%	48%	2%	1.032
Body centered cubic	8	68%	32%	18%	1.286
Extended SC	10	52%	48%	2%	1.032
Face centered cubic	12	74%	26%	24%	1.418

Table 2
Geometric parameters summary for different lattice structures.

Lattice structure	Sphere/pore size ratio (r/R)	Estimated pore radius (R)	Estimated node radius (r)
Simple cubic	1.032	10 μm	10.3 μm
Body centered cubic	1.286	2 μm	2.6 μm
Extended SC	1.032	10 μm	10.3 μm
Face centered cubic	1.418	1 μm	1.4 μm

to the porosity that occurs between the nodes in an undisturbed lattice, or the micro-porosity. In the following sections we will combine the micro-porosity found in Section 2.2, with the porosity information from Fig. 6, along with the sphere or node radius Eq. (4) to arrive at the estimated sphere radius associated with each of the lattice structures. The nominal pore radius, and estimated sphere radius for the various lattice structures are determined in the following sections and summarized in Table 2 in Section 3.5.

3.1. Calculating macro-pore size percentages

In this paper, micro-pores are considered to be the volume between connected spheres and will have no influence on the conductivity of the overall reactant/product system because they do not modify the lattice structure. Conversely, macro-pores are defined as pores equal to or greater than the size of the nodes in the model. Because the void volume is not conductive and reduces the conductivity of the system, macro-pores are modeled as if they were nonconductive additives in varying sizes. For macro-pores on the same size order as the spheres, a single node (1 node radius) is marked always nonconductive. For larger nodes, double sized (2 node radius) or quadruple sized (4 node radius) groups are similarly marked. We turn to Fig. 6 to determine the proper amounts of each group to remove.

To properly calculate the total percentage of the nodes to be removed from the lattice, we must consider that the structure already has micro-porosity. The true macro-porosity in the lattice is simply the difference between the final porosity and the micro-porosity (i.e. $\varepsilon_F - \varepsilon_\mu$), however; this is not the fraction of nodes to be removed from the lattice. In order to not count the micro-porosity twice for those nodes being removed, the macro-porosity, ε'_M, as calculated above must be scaled by the packing factor:

$$\varepsilon'_M = \frac{\varepsilon_F - \varepsilon_\mu}{PF} \quad (8)$$

where ε'_M is the macro-porosity (percentage of nodes to be removed), ε_F the final porosity and ε_μ the micro-porosity.

We discuss the calculations for each lattice in the following sections. A summary of the results including effective pore radii and node percentage removed are found in Tables 2 and 3 in Section 3.5.

3.2. Estimated XSC sphere size and macro-porosity

The nominal pore size for the XSC structure occurs at the pore radius equal to the micro-porosity. In the XSC lattice structure, the micro-porosity is 48% (see Section 2.2). This leaves 2% macro-porosity in a 50% porous electrode. In other words, 4% of the total pore volume is larger than the nominal pore radius for an undisturbed XSC lattice. From the data presented in Fig. 6, we see that the nominal pore radius, $R_{xsc,}$ for the XSC lattice structure is about 10 μm. The approximate sphere radius for XSC from Eq. (4) is $r_{xsc} = 1.032R_{xsc} = 10.3$ μm.

The task at hand is to find the total number of each size of macro-pore to bring the final porosity to 50% in the XSC lattice structure. As noted in Section 2.2, the micro-porosity already present in this lattice structure is 48%, which leaves only 2% in macro-porosity. From Eq. (8), we find that the total fraction of nodes to be removed from the XSC lattice is about 4%. As discussed above, we calculated the XSC node size to be slightly larger than 10 μm. Using Fig. 6, we see that about 2% of the macro-porosity is 10.3 μm (1 node radius) macro-pores and the remaining 2% is 20.6 μm (2 node radius) macro-pores.

3.3. Estimated BCC sphere size and macro-porosity

The nominal pore size for the BCC structure occurs at the pore radius equal to the micro-porosity. In the BCC lattice structure, the micro-porosity is 32% (see Table 1). This leaves 18% macro-porosity in a 50% porous electrode. In other words, 36% of the total pore volume is larger than the nominal pore radius for an undisturbed BCC lattice. From the data presented in Fig. 6, we see that the nominal pore radius, $R_{bcc,}$ for the BCC lattice structure is about 2 μm. The approximate node radius for the BCC structure from Eq. (4) is $r_{bcc} = 1.286R_{bcc} = 2.6$ μm.

We now need to calculate the percentages of the macro-pores to bring the final porosity to 50% in the BCC lattice structure. From Table 1, the micro-porosity present in this lattice structure is 32%, which leaves 18% for the macro-porosity. Again applying Eq. (8), we find the total fraction of nodes to be removed from the BCC lattice as about 27%. The BCC node size is about 2.6 μm so using Fig. 6, the 27% that must be removed has 12% of the 2.6 μm (1 node radius) macro-pores, 9% for the 5.2 μm (2 node radius) macro-pores, and 6% for the 10.4 μm (4 node radius) macro-pores.

3.4. Estimated FCC sphere size and macro-porosity

The nominal pore size for the FCC structure occurs at the pore radius equal to the micro-porosity. In the FCC lattice structure, the micro-porosity is 26% (see Section 2.4). This leaves 24% macro-porosity in a 50% porous electrode. In other words, 48% of the total pore volume is larger than the nominal pore radius for an undisturbed FCC lattice. From the data presented in Fig. 6, we see that the nominal pore radius, $R_{fcc,}$ for the FCC lattice structure is about 1 μm. The approximate node radius for the FCC structure from Table 1 is $r_{fcc} = 1.418R_{fcc} = 1.4$ μm.

Table 3
Macro-porosity and node size for different lattice structures (3D model).

Lattice value	SC–XSC		BCC		FCC	
	Pore radius	Percent removed	Pore radius	Percent removed	Pore radius	Percent removed
1 × 1	10.3 μm	2%	2.6 μm	12%	1.4 μm	15%
2 × 2	20.6 μm	2%	5.2 μm	9%	2.8 μm	11%
4 × 4	41.2 μm	0%	10.4 μm	6%	5.6 μm	7%
Total		4%		27%		33%

Table 4
Critical volume fraction of different lattice structures with 50% porosity.

Lattice structure	Estimated sphere radius (r)	Critical percolation probabilities	Utilization of 3D model with micro-porosity	Utilization of 3D model with 50% porosity
Simple cubic ($z=6$)	10.3 μm	0.67–0.71	0.651	0.596
Body centered cubic ($z=8$)	2.6 μm	0.74–0.78	0.746	0.604
Extended cubic ($z=10$)	10.3 μm	No results (not realizable)	0.759	0.670
Face centered cubic ($z=12$)	1.4 μm	0.795–0.815	0.795	0.608

Finally, we find the total number of each macro-pore size so that the final porosity of 50% is achieved in the FCC lattice structure. From Table 1, the micro-porosity present is only 26%, which leaves 24% for the macro-porosity. Applying Eq. (8) once more yields the total fraction of nodes to be removed from the FCC lattice as 33%. From Fig. 6, we divide the 33% to be removed into 15% for the 1.4 μm ($1\times1\times1$) macro-pores, 11% for the 2.8 μm ($2\times2\times2$) macro-pores, and 7% for the 5.6 μm ($4\times4\times4$) macro-pores.

3.5. Summary of macro-porosity and node size

In the previous sections, the calculations relating pore radius to sphere radius and node removal to achieve 50% porosity were presented. Table 2 summarizes the approximate pore radius found in the various structures and the correlating sphere radius. For both the SC and the XSC structures the approximate sphere radius is 10.3 μm. For the more densely packed structures, the estimated sphere radius is smaller; 2.6 μm for BCC and 1.4 μm for FCC.

Table 3 provides information on the macro-porosity and node size distribution for the different lattice structures. Note that the SC and XSC have the same structure and macro-porosity distribution. The percent of nodes removed for the SC and XSC is only 4%. The percent of nodes removed for the BCC and FCC is 27% and 33%, respectively. All these structures have a total porosity of 50% and these structures will be analyzed in the next section to determine their critical volume fraction (CVF).

4. Critical volume fraction (CVF) simulation results

With the structures complete, we determined the CVF for each structure using the 3D conductivity model [8,9,10]. However, we first verified the model by comparing the results of the 3D conductivity model with established percolation theory data. Then the model was run with the macro-porosity included to model the effects of porosity. The results are presented in the next three sections. The simulation results, along with the theoretical values are listed in Table 4 for comparison.

The number of nodes and the size of the model determine the accuracy of the computer simulation. A large array will give accurate results. However, if the array is too large then the model either takes too long to execute or crashes the computer running the model.

The final size of the array of nodes modeled in this paper was $1024\times1024\times17$, which is the number of nodes used in previous papers [8,9,10]. This represents over 17 million nodes to sort through. We ran all the simulations on the "cluster" of computers in the Microelectronics Research and Communications Institute at the University of Idaho. Each computer has 4G RAM and Dual Pentium IV 3.4 GHz CPUs and it took several hours to run each simulation. When more than 17 layers were used to simulate the thickness of the electrode, the program running time increased (for 20 layers the execution time doubled), but the difference of the utilization was within 0.1%. From these results, we concluded that the 17 layer simulation results provided sufficient accuracy.

4.1. SC–XSC simulation results

We can compare the CVF from the computer simulation with the theoretical values when the electrodes have no macro-porosity. For the SC structure, the model with no macro-porosity converged to 65.1% utilization which matched well with the critical percolation probability predicted by the percolation theory [14], which gives 0.69 ± 0.02. One will note that the XSC structure has no theoretical percolation probability due to the non-symmetric distances (i.e. the structure is not physically realizable), however; for comparison, the XSC with the higher coordination number $z=10$ yielded 75.9% utilization. The theoretical discharge limit, or the critical volume fraction, that was predicted by running the 3D conductivity model including the macro-pores represented by nonconductive additives gave 59.6% for SC and 67.0% for XSC.

4.2. BCC simulation results

For the BCC model the simulation was again conducted with and without macro-porosity to verify the model. The BCC structure with no macro-porosity converged to 74.6% utilization. This also matched well with the critical percolation probability of 0.76 ± 0.02 predicted by the percolation theory [14]. The theoretical discharge limit as returned with the 50% porous BCC model was 60.4%.

4.3. FCC simulation results

The FCC model simulation was conducted with and without macro-porosity in a similar manner to what was done for the other models. For the FCC structure without macro-porosity, the model converged to 74.6% utilization, which again matched well with the critical percolation probability of 0.76 ± 0.02 predicted by the percolation theory [14]. The theoretical discharge limit was 60.8% for the FCC model with 50% porosity.

4.4. Summary of simulation results

The conductivity simulation results are found in Table 4. The utilization of the different lattice structures having only micro-porosity (i.e. no macro-porosity) represents the maximum CVF achievable by each of the lattices. The maximum CVF possible is 0.795 and occurs with the FCC lattice structure. As macro-porosity is added to provide a total porosity of 50%, the CVF is reduced. As stated before, the extended simple cubic structure is not realizable in real world condition. As a result, the utilization for this structure does not follow the pattern set by the realizable structures. The increase in the number of connections for the extended cubic structure ($z=10$) over the simple cubic structure ($z=6$) caused the utilization to increase from 59.6% to 67.0% when the total porosity is 50%. For all the realizable structures evaluated in this paper when the total porosity is 50%, the critical volume fraction was 0.603 ± 0.007, which matches closely with the 2D value reported previously [8].

5. Conclusions

In this paper, theoretical models independent of the electrochemical system are derived for different lattice structures. These structures consist of electrically conductive nodes all having the same size connected together in the specified arrangement of the lattice. As the electrode undergoes a reaction, these nodes change from being conductive to nonconductive. The extent to which this theoretical model can be applied to a given electrode is dependent on the specific characteristics of that electrode.

An important result is that the node size for the positive electrode of a lead acid battery was estimated from its porosity distributions for three lattice structures: extended simple cubic (XSC), body centered cubic (BCC), and face centered cubic (FCC). The node size can be estimated because any pore smaller than a single node is counted as part of the micro-porosity that exists between the nodes in the model. Porosity larger than the single node size, the macro-porosity, is modeled with nonconductive additives having the same pore size as the porosity being modeled. This approach is used to determine both the sphere or node size in the model as well as the influence of porosity on the critical volume fraction. We showed that under these assumptions, the micro-porosity for extended simple cubic (XSC) to be 48%; for body centered cubic (BCC), 32%; and for face centered cubic (FCC), 26%. These micro-porosity values translate to node sphere sizes in the 1–10 μm range as given in Table 4.

Using previous experimental data from other investigators, we were able to estimate the distribution of the macro-porosity for the different structures. This distribution was based on a total plate porosity of 50%. A 3D conductivity model was then used to estimate the critical volume fraction (CVF) for all the structures based on their macro-porosity distribution. The CVF for the simple cubic, body centered cubic, extended simple cubic, and face centered cubic was 0.596, 0.604, 0.670, and 0.608, respectively. It is interesting to note that the CVF for all the physically realizable structures was 0.603 ± 0.007, which is very close to the estimated two-dimensional CVF and to experimental data. The extended simple cubic model where the coordination number z is ten cannot be physically assembled with the diagonal nodes touching the center node.

Previous research [3] has indicated that the statistical average for the coordination number of the positive active material in lead acid batteries is approximately $z = 8$, a claim which is supported by this work. This coordination number is the same as the BCC structure. A BCC structure having only micro-porosity (i.e. 32%) has a CVF of 74.6% as estimated by the 3D conductivity model. This value compares favorably with the percolation value of 74–78%. When the macro-porosity is included in the model so that the total plate porosity is 50%, the utilization of the BCC structure is 60.3%, which compares favorably to experimental results.

In reality, battery plates are composed of small particles in various sizes packed in a variety of lattice structures. A model which only uses one lattice structure and one node size would appear to be an oversimplification of a very complex arrangement. However, the critical volume fractions (CVFs) for all the physically realizable structures (i.e. SCC, BCC, and FCC) were all close to 0.60 when the total porosity was 50%. The estimated node size for all these realizable structures were also similar and varied from about 1 to 10 μm. This suggests that a plate's complex arrangement may be modeled by summing all the different realizable lattice structures with their corresponding node sizes because they all provide the same approximate CVF result.

Acknowledgements

The authors gratefully acknowledge the support of the Office of Naval Research, which has supported this work under the award "Advanced Lead Acid Battery Development for Military Vehicles" No. N00014-04-1-0612.

References

[1] H. Bode, Lead-Acid Batteries, John Wiley & Sons, New York, 1977, pp. 297-303.
[2] H. Metzendorf, J. Power Sources 7 (1982) 281–291.
[3] K.-J. Euler, R. Kirchhof, H. Metzendorf, J. Power Sources 5 (1980) 255–262.
[4] D. Stauffer, A. Aharony, Introduction to Percolation Theory, revised 2nd edition, Taylor & Francis, 1994.
[5] S. Kirkpatrick, Phys. Rev. Lett. 27 (1971) 1722–1725.
[6] D. Pavlov, J. Electrochem. Soc. 139 (1992) 3075, doi:10.1149/1.2069034.
[7] D.B. Edward, S. Zhang, J. Power sources 135 (2004) 297–303.
[8] D.B. Edwards, S. Zhang, J. Power Sources 158 (2006) 927–931.
[9] D.B. Edwards, S. Zhang, J. Power Sources 172 (2007) 957–996.
[10] S. Zhang, Investigating paste additives to improve the specific energy performance of lead-acid batteries, Dissertation, University of Idaho, Moscow, ID, USA, 2005.
[11] E.E. Ferg, P. Loyson, N. Rust, J. Power Sources 141 (March(2)) (2005) 316–325.
[12] E.E. Ferg, L. Geyer, A. Poorun, J. Power Sources 116 (July(1–2)) (2003) 211–218.
[13] D. Pavlov, M. Dimitrov, T. Rogachev, L. Bogdanova, J. Power Sources 114 (February(1)) (2003) 137–159.
[14] H. Scher, R. Zallen, J. Chem. Phys. 53 (1970).